








Sequence-dependent mechanochemical coupling of helicase translocation and unwinding at single-nucleotide resolution

Andrew H. Laszlo^{a,1} , Jonathan M. Craig^a , Momčilo Gavrilov^b , Ramreddy Tippana^b, Ian C. Nova^a, Jesse R. Huang^a , Hwanhee C. Kim^a, Sarah J. Abell^a, Mallory deCampos-Stairiker^a, Jonathan W. Mount^a, Jasmine L. Bowman^a, Katherine S. Baker^a, Hugh Higinbotham^a, Dmitriy Bobrovnikov^b, Taekjip Ha^b , and Jens H. Gundlach^a

Edited by Michelle Wang, Cornell University, Ithaca, NY; received February 11, 2022; accepted August 2, 2022 by Editorial Board Member Stephen J. Benkovic

We used single-molecule picometer-resolution nanopore tweezers (SPRNT) to resolve the millisecond single-nucleotide steps of superfamily 1 helicase PcrA as it translocates on, or unwinds, several kilobase-long DNA molecules. We recorded more than two million enzyme steps under various assisting and opposing forces in diverse adenosine tri- and diphosphate conditions to comprehensively explore the mechanochemistry of PcrA motion. Forces applied in SPRNT mimic forces and physical barriers PcrA experiences *in vivo*, such as when the helicase encounters bound proteins or duplex DNA. We show how PcrA's kinetics change with such stimuli. SPRNT allows for direct association of the underlying DNA sequence with observed enzyme kinetics. Our data reveal that the underlying DNA sequence passing through the helicase strongly influences the kinetics during translocation and unwinding. Surprisingly, unwinding kinetics are not solely dominated by the base pairs being unwound. Instead, the sequence of the single-stranded DNA on which the PcrA walks determines much of the kinetics of unwinding.

single-molecule | force spectroscopy | helicase | DNA | SPRNT

Helicases are involved in nearly every aspect of nucleic acid metabolism throughout the tree of life. A full picture of their mechanochemical action is currently missing because of the difficulty of observing the small, fast steps taken by helicases. Helicases use repeated cycles of adenosine triphosphate (ATP) hydrolysis to generate directed inchworm-like motion along a single-stranded (ss) nucleic acid and thereby unwind nucleic acid duplexes and remove bound proteins (1–4), performing key roles during replication, transcription, and translation of nucleic acids. Biophysical approaches (5), such as X-ray crystallography (6), single-molecule fluorescence resonance energy transfer (7), optical tweezers (8–12), and magnetic tweezers (13), have shed light on helicase mechanisms, yet understanding of the mechanochemical choreography of translocation and unwinding is incomplete, in part because helicases take small steps (<0.6 nm) at high speed (~1 step/ms), which is beyond the resolution of most single-molecule techniques.

Single-molecule picometer-resolution nanopore tweezers (SPRNT) (Fig. 1) is a technique for measuring the activities of nucleic acid-processing enzymes at high spatiotemporal resolution (14, 15). SPRNT records the motion of ss nucleic acid as a motor enzyme feeds it through a *Mycobacterium smegmatis* porin A (MspA) nanopore (Fig. 1A, *Materials and Methods*). A voltage applied over the nanopore causes an ion current through the pore and applies an electrophoretic force to the DNA. As the motor enzyme draws DNA through the pore, different bases within the pore block the pore to differing degrees and thereby characteristically affect the ion current. The procession of ion current values is used to determine the nucleic acid sequence, which serves as the basis for nanopore sequencing (16, 17). This signal also provides a record of the enzyme's position on its nucleic acid substrate at exquisite spatiotemporal resolution (14, 15). Put simply, SPRNT measures an enzyme's location along a DNA strand by simply reading off the DNA sequence as it is moved through the pore, just as one would read the ticks on a ruler.

SPRNT is capable of resolving subnucleotide nucleic acid motion on submillisecond timescales (14, 15) over distances of thousands of nucleotides while simultaneously revealing the enzyme's sequence-specific location. SPRNT has high throughput, enabling the collection of large datasets across a broad range of experimental parameters (18). SPRNT also applies a force to the motor enzyme, which can be used to probe force-generating substeps. Previously, we demonstrated SPRNT using opposing forces to enzymes translocating on ssDNA (14, 18–20) (Fig. 1B, *i*). Here, we expand its use to include assisting forces (Fig. 1B, *ii*) and to observe duplex unwinding with SPRNT (Fig. 1B, *iii*).

Much of what is known to date about how helicases walk along and unwind DNA comes from studies of the superfamily (SF) 1 helicase PcrA and homologs such as Rep

Significance

DNA helicases use the energy of adenosine triphosphate hydrolysis to walk along and unwind DNA, making them essential for many cellular tasks. Still, key details of how they work are not well understood, because their small (0.6 nm) and fast (~1 ms) steps make them difficult to study using traditional biophysical approaches. Here, we apply nanopore tweezers, which is capable of clearly resolving these steps, to shed light on how a prototypical helicase called PcrA works. By changing different aspects of the nanopore tweezers experiment, we probe different substates of the ATPase cycle. Nanopore tweezers provides an enzyme's sequence-specific location and surprisingly reveals that the underlying single-stranded DNA sequence strongly affects the ability of PcrA to unwind double-stranded DNA.

Author contributions: A.H.L., J.M.C., I.C.N., T.H., and J.H.G. designed research; A.H.L., J.R.H., H.C.K., S.J.A., M.d.-S., J.W.M., J.L.B., K.S.B., and H.H. performed research; A.H.L., M.G., R.T., D.B., and T.H. contributed new reagents/analytic tools; A.H.L. analyzed data; and A.H.L., T.H., and J.H.G. wrote the paper.

The authors declare a competing interest. The University of Washington has filed a patent on the SPRNT technology.

This article is a PNAS Direct Submission. M.W. is a Guest Editor invited by the Editorial Board.

Copyright © 2022 the Author(s). Published by PNAS. This article is distributed under Creative Commons Attribution-NonCommercial-NoDerivatives License 4.0 (CC BY-NC-ND).

¹To whom correspondence may be addressed. Email: laszloa@uw.edu.

This article contains supporting information online at <http://www.pnas.org/lookup/suppl/doi:10.1073/pnas.2202489119/-/DCSupplemental>.

Published August 29, 2022.

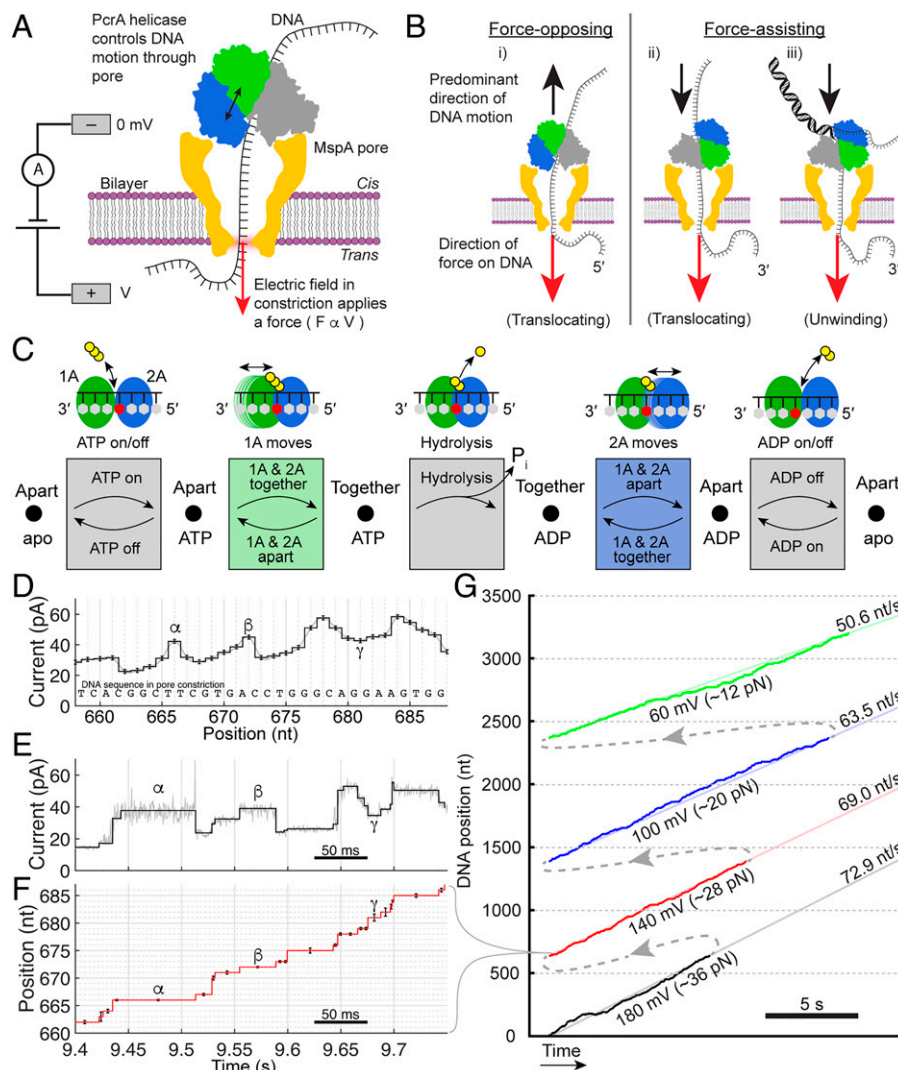


Fig. 1. SPRNT analysis of PcrA. (A) SPRNT measures the progression of DNA nucleotides through a protein nanopore. DNA bases are identified within the pore constriction by their characteristic ion current and their progression can be used to monitor the progression of a helicase along a DNA strand. RecA-like walker domains 1A and 2A are highlighted in green and blue, respectively. (B) Various experimental configurations used to probe different aspects of helicase motion in force-opposing and force-assisting configurations. Force-opposing unwinding is not possible with SPRNT because the MspA constriction is only wide enough for ssDNA. (C) Inchworm kinetic model of SF1 and SF2 helicases consists of a series of enzyme states (dots) connected by physical and chemical substeps (arrows). The substeps, in order of occurrence, are 1) ATP binding and unbinding; 2) domain 1A sliding forward and backward as the helicase closes/opens, respectively; 3) ATP hydrolysis; 4) domain 2A sliding forward and backward as the helicase opens and closes, respectively; and 5) ADP release. In principle, each step has a forward and backward rate; however, here we treat hydrolysis as irreversible since the concentration of inorganic phosphate is effectively zero. (D) Segment of consensus ion-current levels. As the DNA strand is fed through the nanopore, DNA bases within the pore produce different currents, allowing them to be identified. (E) Example raw ion-current data as a single PcrA helicase translocates along the DNA bases shown in D at [ATP] = 1,000 μ M. (F) Aligned position within the repeat DNA strand for the data shown in E. Greek letters α , β , and γ have been added within panels D-F, indicating particular steps within the sequence. (G) Zoom out of aligned SPRNT data shown in F. The applied voltage (force) is successively changed, resulting in changes in the observed helicase stepping rate. F, force; V, voltage.

and UvrD (6, 21–26). PcrA has two RecA-like domains, domain 1A and domain 2A, that individually bind to ssDNA (6). Between these two domains lies a highly conserved ATP-binding pocket. PcrA translocates along the DNA lattice by progressing through a series of kinetic substates that are connected by either chemical or physical substeps (6, 22) (Fig. 1C). ATP binding induces a conformational change in the protein, bringing 1A and 2A closer together. Then, hydrolysis of ATP to adenosine diphosphate (ADP) allows for a conformational relaxation of the protein, followed by ADP release. During the ATPase cycle, either 1A or 2A slide along the DNA backbone in alternating fashion, a so-called inchworm mechanism (6), resulting in directed motion along the DNA. Fig. 1C shows a schematic of the inchworm mechanism consisting of several states, separated by chemical and physical substeps between those states.

SF1 and SF2 helicases are thought to walk in similar manners because they share many core motifs for nucleic acid binding, nucleotide-triphosphate binding, and nucleotide-triphosphate hydrolysis (2, 3, 5, 6, 27–30). While wild-type (WT) PcrA is not particularly processive in unwinding, PcrA can be activated into a highly processive helicase “PcrA-X” by locking it into its active conformation via chemical crosslinking (31) (*Materials and Methods*). We use this activated form of PcrA here to better understand PcrA’s mechanism of DNA unwinding and, for simplicity, refer to it as PcrA from here onward.

While all of this is certain, it is based on indirect lines of inference and measurement; single ATP-turnover events have yet to be directly observed under physiological conditions for any SF1 helicase in a single-molecule assay, because they are too small and fast to be resolved by most single-molecule assays

other than SPRNT. Our previous SPRNT studies of the SF2 helicase Hel308 translocating along ssDNA revealed that Hel308 fed the DNA through the pore in two physical substeps per nucleotide and revealed the chronology of the chemical substeps (i.e., ATP binding, hydrolysis, and ADP release) and conformational-change substeps that produce processive motion. In Hel308, the DNA sequence, but not the magnitude of the opposing force, strongly influenced translocation kinetics (14, 18–20). Here, we have applied SPRNT to PcrA to test existing models of SF1 translocation and to determine whether the lessons learned from Hel308 can be applied broadly to SF1 and SF2 helicases. We also compare PcrA molecules translocating along ssDNA with those unwinding DNA duplexes, providing insight into the mechanism of DNA unwinding.

Results

We recorded more than 600 single-molecule trajectories of PcrA helicases both unwinding and translocating along a repetitive, ~6-kb-long (32) DNA construct (*Materials and Methods* and *SI Appendix, Figs. S1–S5*) at different ATP and ADP concentrations and with various assisting and opposing forces. The repetitive DNA was made up of 64 repeated sections of 86 nucleotides separated by one of eight 17-base linker segments in the following configuration:

$$(R_{86} - A - R_{86} - B - R_{86} - C - R_{86} - D - R_{86} - E - R_{86} - F - R_{86} - G - R_{86} - H) \times 8,$$

where R_{86} is the 86-base repeat section and A, B, C, and so forth represent the different linker segments (the full sequence is provided in *SI Appendix*). This DNA strand was modified with end adaptors that enabled use in force-opposing (translocase mode only; Fig. 1 *B*, *i*) and force-assisting (translocase and unwinding mode; Fig. 1 *B*, *ii* and *iii*) configurations (*SI Appendix, Figs. S1 and S2*, adaptor sequences in *Table S1*). Use of this strand regularly produced several-kilobase-long single-molecule traces of individual PcrA molecules. In each full 6.6-kb trace, a single PcrA molecule walks over 64 repeated instances of the 86-base repeat sequence and 8 instances of each of the eight linker sequences, allowing for accumulation of significant single-molecule statistics from individual traces. In total, this dataset comprises more than 50 h of helicase-on-pore time, traveling over a combined 2.3 million bases of DNA. This, to our knowledge, represents the largest number of single-enzyme turnover steps analyzed in a single study for any motor protein (*SI Appendix, Tables S2 and S3*).

Because each trace encompasses thousands of individual enzyme turnover events, we were able to change the applied voltage successively during each trace to accumulate single-molecule statistics for each individual PcrA helicase at several different forces. For example, Fig. 1 *G* shows a trace in which an assisting force was changed successively from ~36 pN to ~28 pN to ~20 pN, and finally to ~12 pN, while a single PcrA helicase translocated over a long ssDNA. As force decreased, the observed mean stepping rate also decreased.

Understanding PcrA Motion in SPRNT. In agreement with previous studies of PcrA (6, 21, 33), we observed PcrA take single-nucleotide steps (Fig. 1 *D–F* and *SI Appendix, Figs. S6–S11*). This is in contrast to SPRNT experiments with Hel308 helicase (14), which revealed two approximately half-nucleotide substeps per ATP hydrolyzed (*SI Appendix, Fig. S6*). Control experiments with other SF1 helicases, Rep-X and UvrD, also revealed only

single-nucleotide steps (*SI Appendix, Fig. S12*) in our SPRNT assay. We suspect this difference arises from how PcrA, Rep, and UvrD rest on the pore rim in comparison with Hel308. Proper interpretation of our data requires that we understand which substep(s) of the inchworm mechanism results in motion of the DNA through MspA for these experiments. We previously determined that the two observed substeps per ATP hydrolyzed in Hel308 corresponded to the two conformational-change substeps of the inchworm mechanism (Fig. 1 *C*, motion of domain 1A relative to the DNA and motion of domain 2A relative to the DNA). Shifting of Hel308 on the pore rim, as opposed to a half-nucleotide motion of Hel308 along the DNA strand, is the reason for the apparent half-step motion of DNA through the pore. This suggests that one of these conformational-change substeps is responsible for the single step per ATP observed in PcrA, Rep, and UvrD, while the other conformational-change substep is unobservable.

To determine whether domain 1A motion or domain 2A motion is the observable step in our experiments, we return to the schematic in Fig. 1 *B* (see also a schematic based on crystal structures of MspA and PcrA in *SI Appendix, Fig. S13*). In force-opposing experiments, domain 2A is in contact with the pore rim; however, in force-assisting experiments, domain 1A is in contact with the pore rim. We hypothesize that different substeps are observable depending on which end of the DNA is threaded through the pore (i.e., whether the force is assisting or opposing PcrA motion). This is because SPRNT measures the DNA motion relative to the enzyme surface that is in contact with MspA. That is, in force-opposing experiments, the observable step is motion of domain 2A backward and forward along the DNA (Fig. 2 *A*), whereas in force-assisting experiments, the observable step is motions of domain 1A along the DNA (Fig. 2 *B* and *C*). This is confirmed in the data that follow.

Fig. 3 *A* and *B* summarizes the average speed at each force, ATP, and ADP condition. As expected, larger opposing forces slowed the motion of PcrA, while larger assisting forces sped it up; reduction in ATP concentration or an increase in ADP concentration lowered the average speed. Interestingly, the average speed was lower at ~12 pN assisting force than at ~12 pN opposing force, possibly due to slight distortions of the helicase that depend on how it rests on the pore rim. The range of speeds observed was quite broad; however, individual enzymes had tighter speed distributions than the combined dataset (*SI Appendix, Fig. S14*). In other words, there exist individual enzymes that were consistently faster or slower than average, a phenomenon known as static disorder, possibly caused by slightly different folding states or oxidative damage (34–36). For comparison with previously published measurements (21, 31, 37), Michaelis–Menten curves and inhibition curves for each applied force are shown in *SI Appendix, Fig. S15*. Translocation and unwinding rates are in agreement with those reported previously. Maximum velocity (V_{\max}) was much lower for unwinding than for ssDNA translocation (14 ± 3 nucleotides [nt]/s vs. 55 ± 6 nt/s, SEM), presumably because base-pair unwinding is rate limiting. Accordingly, saturation occurred at a lower ATP concentration for unwinding experiments ($K_M = 1.5 \pm 1.1$ μ M at ~28 pN assisting force, SEM) compared with ssDNA translocation ($K_M = 6.4 \pm 1.8$ μ M at ~28 pN assisting force, SEM).

In unwinding experiments, some stepping was observed at zero ATP concentration ([ATP]) (*SI Appendix, Fig. S16*). We attribute this to off-pathway, diffusive motion of the enzyme along the DNA that is rectified by the assisting force. Forward steps with assisting force are then some combination of 1) on-pathway steps, as in Fig. 2; and 2) force-driven, off-pathway steps.

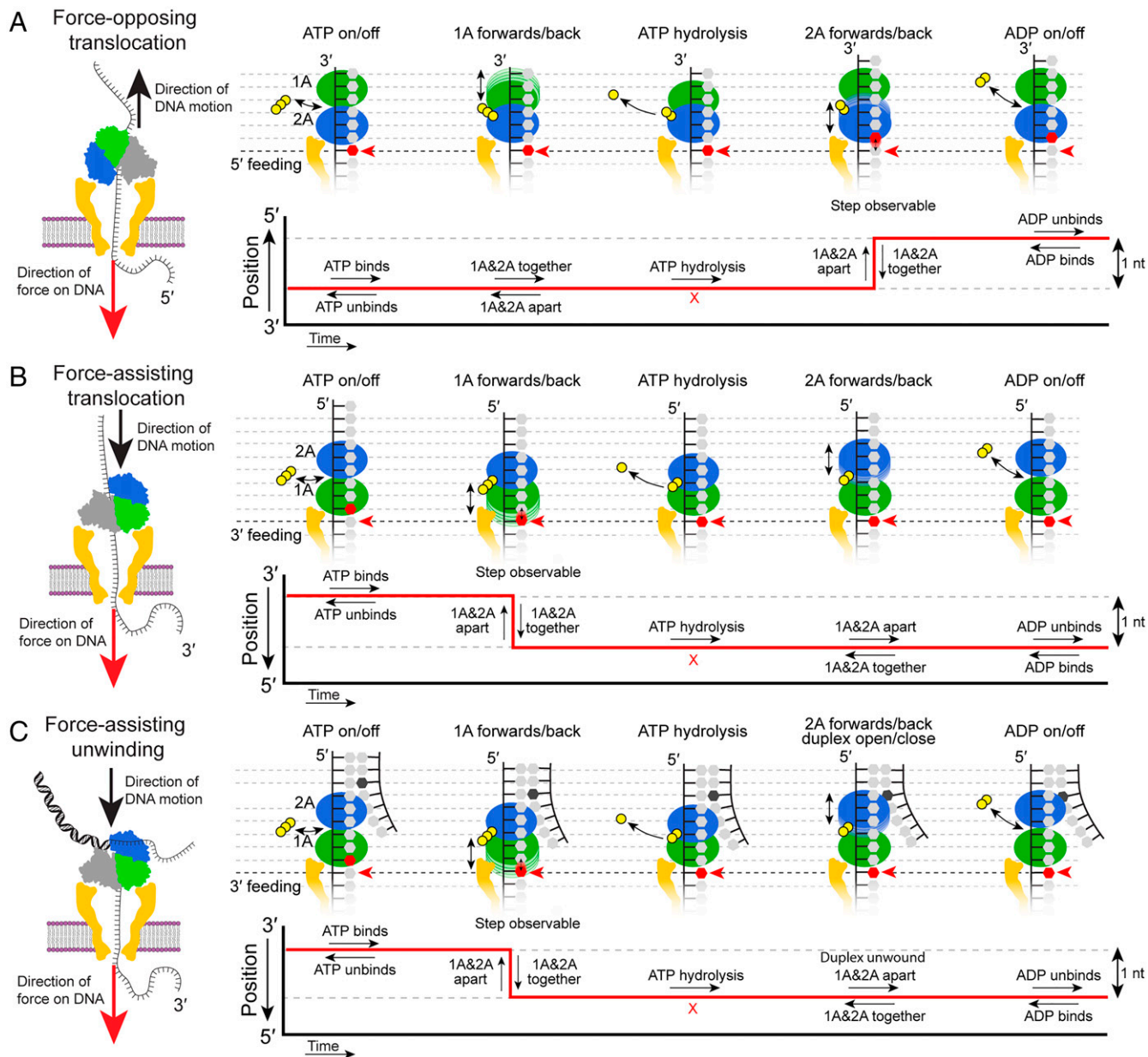


Fig. 2. Kinetic model for PcrA translocation and unwinding in the context of SPRNT. (A) Force-opposing translocation: kinetic model from Fig. 1A in the context of SPRNT with the 5' end of the substrate DNA fed into the pore. (Right) The observable step occurs as the helicase transitions between "together" and "apart" and domain 2A slides along the DNA. (Right, Bottom) In red, a schematic SPRNT data trace showing where in the ATPase cycle the observable step occurs. (B) Force-assisting translocation: kinetic model from Fig. 1A in the context of SPRNT with the 3' end of the substrate DNA fed into the pore. (Right) The observable step occurs as the helicase transitions between the "apart" and "together" state with domain 1A sliding along the DNA. (Right, Bottom) In red, a schematic data trace showing where in the ATPase cycle the observable step occurs. (C) Force-assisting unwinding: As with force-assisted translocation, the forward and backward motion of domain 1A is the observable step, while unwinding of the complementary strand occurs either immediately prior to or coincident with domain 2A's advance. Because of the irreversibility of the ATP hydrolysis step (inorganic phosphate concentration = 0), ADP is only able to directly drive backstepping in 5' feeding experiments. High [ADP] instead increases observed step duration in force-assisting experiments. Off-pathway steps such as diffusive, [ATP]-independent movement are omitted for simplicity.

We account for this effect with a modified Michaelis–Menten equation of the form:

$$R = \frac{V_{max} * [ATP]}{K_M + [ATP]} + C,$$

which includes the normal Michaelis–Menten term with the addition of an [ATP]-independent constant C, where C is determined by the stepping rate at [ATP] = 0 (SI Appendix, Fig. S15). Put simply, the total rate, R, is the sum of the on-pathway rate and off-pathway rate. The ratio of C to R yields the fraction of the observed steps that are off-pathway at each applied force. Intriguingly, during unwinding, only C increases with force, while the

V_{max} , which is associated with ATP hydrolysis-driven motion, remains constant (SI Appendix, Fig. S15). This suggests that only off-pathway steps are affected by the assisting force, while on-pathway ATP hydrolysis-driven unwinding is not affected by force. This is because force applied during SPRNT couples only to steps that result in motion of DNA through the pore, since the applied force on the DNA can only do work on the system when the force results in a change in DNA position (38). This is consistent with the model presented above. In force-opposing experiments, force modifies the forward and backward rates of domain 2A along DNA (Fig. 2A), while in force-assisting experiments, force affects the forward and backward rates of domain

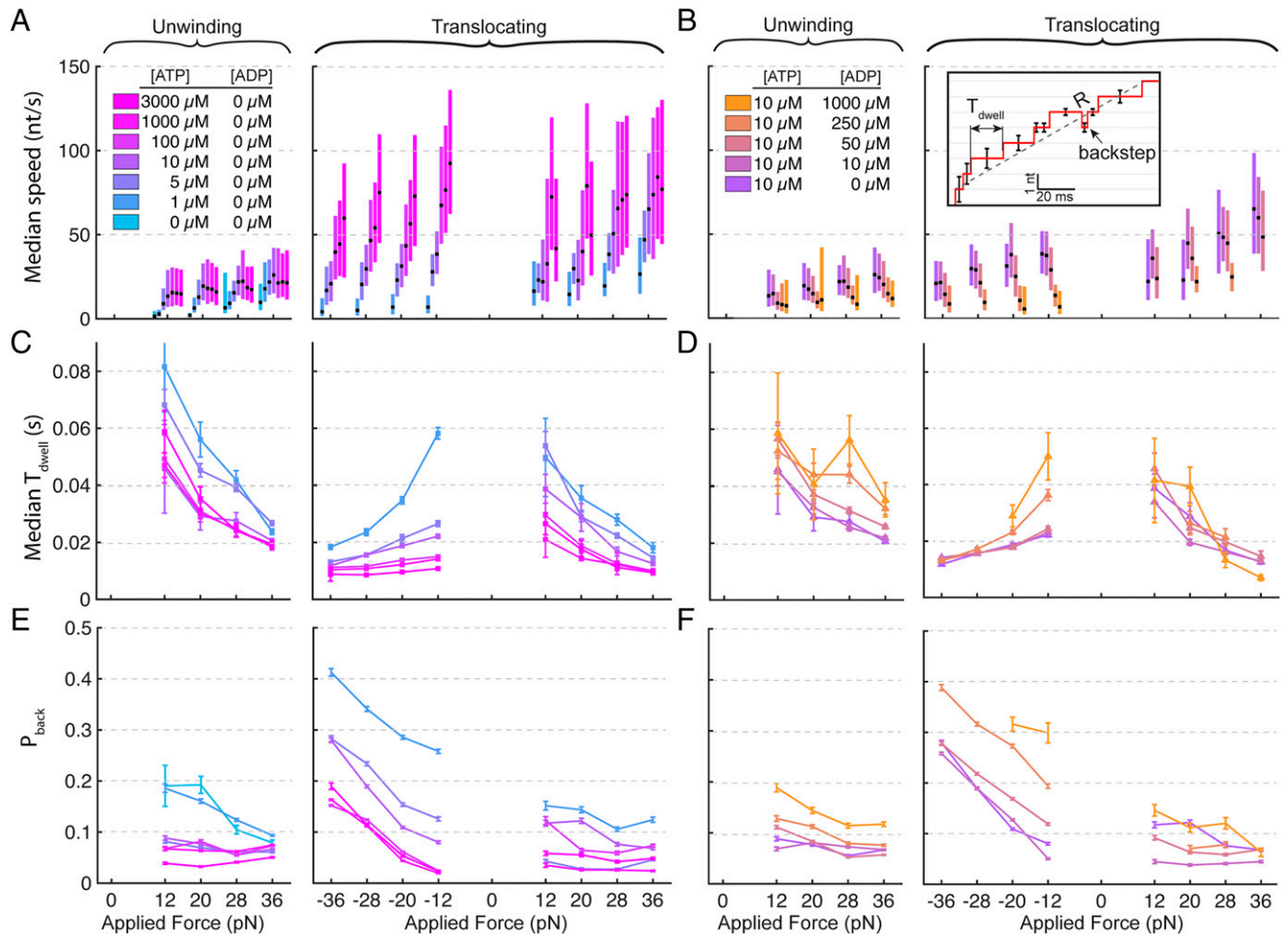


Fig. 3. PcrA stepping kinetics at varying ATP and ADP concentrations. (A and B) Average speed for helicases in various ATP and ADP conditions at all applied forces. The speed was calculated as the average velocity taken over successive 15 nt-long stretches. The black line in the middle of each bar is the median speed; the bars in A and B extend to 25th and 75th percentiles and represent the spread in observed speed across several helicases. Positive forces are assisting, negative forces are opposing. In A, only the unwinding data include an [ATP] = 0 data point; the lowest [ATP] in the translocation data is 1 μ M. (C) Median dwell time as a function of applied force at various ATP concentrations. (D) Median dwell time as a function of force at ATP 10 μ M and various ADP concentrations. (E) Average probability of a backward step as a function of applied force at various ATP concentrations. (F) Probability of a backward step as a function of force at ATP 10 μ M and various ADP concentrations. Inset graphs within each panel demonstrate features of the data being measured: speed, step dwell time, and probability of backstepping [$N_{\text{back}}/(N_{\text{forward}} + N_{\text{back}})$]. For the 36 pN and 28 pN force-opposing [ATP] = 10 μ M, [ADP] = 1,000 μ M condition, the data points were omitted since backstepping was so prevalent (SI Appendix, Fig. S17) that automated alignment was unreliable.

1A (Fig. 2 B and C). Because unwinding is significantly slower than translocation, it is reasonable to suppose that the rate-limiting substep is the one in which duplex unwinding occurs. Because domain 2A advance is rate limiting, force-driven changes in domain 1A motion should have little effect on the rate of on-pathway unwinding.

At each condition, steps of one nucleotide forward or backward were the most prevalent step size observed (SI Appendix, Figs. S10 and S11). While steps larger than one nucleotide were observed, they occurred more often at lower force, where SPRNT resolution is reduced, suggesting that steps larger than one nucleotide are made up of successive, unresolved single-nucleotide steps. For simplicity, we focus the rest of our analysis on single-nucleotide steps. SPRNT's ability to resolve most single-nucleotide steps taken enables us to see the underlying kinetic details, such as dwell-time (Fig. 3 C and D) and backstepping probability (Fig. 3 E and F), and to observe how these observable details give rise to average behavior. For example, as the opposing force was increased, the median dwell time at each nucleotide step during ssDNA translocation decreased. On its own, this is surprising, as one might expect the opposite, since the average speed decreased with opposing force. This apparent

paradox is resolved by noting that the probability of a backstep (P_{back}) increased significantly with opposing force. Thus, opposing force reduces PcrA's average speed by increasing domain 2A's propensity for backstepping rather than simply reducing the forward stepping rate.

As expected, reduced [ATP] led to increased dwell times at all applied forces. Surprisingly, reduced [ATP] also led to increased P_{back} at all applied forces. The inchworm mechanism does not predict that insufficient ATP will cause backward steps, so we attribute this motion to off-pathway behavior, consistent with diffusive motion along the DNA as is seen with higher assisting forces. Such diffusion may generally occur at a low rate and only become visible when low [ATP] or high opposing force sufficiently inhibit on-pathway behavior.

To understand the effect of ADP concentration ([ADP]) on PcrA kinetics, we held [ATP] at 10 μ M while titrating [ADP] up to 1,000 μ M. As [ADP] was increased, the average speed reduced linearly with [ADP], consistent with competitive inhibition of ATP binding. At the level of individual enzyme steps, force-assisting and force-opposing data are remarkably different. In force-opposing experiments, increased [ADP] causes a significant increase in backstepping. At higher opposing forces

(≥ 28 pN) and $[ADP] = 1,000 \mu\text{M}$, backstepping was so prevalent as to render alignment to the DNA sequence impossible (*SI Appendix, Fig. S17*). In contrast, in force-assisting experiments, little change in P_{back} was observed with changing $[ADP]$. This discrepancy can be understood by looking at the model in Fig. 2. The presence of ADP should allow for backstepping of domain 2A, which is observable during force-opposing experiments. However, because the concentration of inorganic phosphate is essentially zero, hydrolysis is effectively irreversible. Therefore, backstepping of domain 1A, which is the observable step in force-assisting experiments, is unaffected by the presence of ADP. While assisting force measurements are essentially blind to forward and backward motions of domain 2A, these backsteps should instead manifest in the data as longer dwell times, as is apparent in the unwinding data shown in Fig. 3D. Step dwell times for force-assisting translocation do not appear to be significantly longer at high $[ADP]$, suggesting ADP-driven backstepping of domain 2A requires a force opposing PcrA's motion, such as the nanopore rim in force-opposing experiments or the DNA duplex in force-assisting unwinding experiments. Force-opposing data are consistent with this interpretation: as opposing force goes to zero, P_{back} for domain 2A becomes small.

This insight also sheds light on the kinetics of PcrA during unwinding and suggests that opposing force applied during SPRNT is analogous to the opposing force applied by a DNA duplex during unwinding. During force-opposing translocation experiments, numerous backsteps are observed, especially with larger opposing forces. By analogy, we hypothesize that during unwinding, domain 2A makes several attempts to invade the DNA duplex before successfully stepping forward. More attempts are made if the energy barrier is high, either via higher opposing force or a stronger DNA duplex. The unbinding of ADP ultimately rectifies the forward step of domain 2A. A similar mechanism for unwinding has been proposed for NS3 helicase, in which the presence or absence of ATP alters the energy landscape of the helicase on DNA between weakly bound and tightly bound states, respectively (39). Here, both domain 1A and 2A are tightly bound in the *apo* state, then when ATP is bound, domain 2A anchors PcrA in place while Brownian fluctuations of domain 1A back and forth are rectified by ATP hydrolysis. Then with ADP bound, domain 1A anchors PcrA in place while domain 2A undergoes Brownian fluctuations forward and backward along the DNA strand, which are ultimately rectified in the forward-tracked state after ADP unbinding. Comparison of conditional dwell-time distributions further support this interpretation (*SI Appendix, Fig. S18*).

DNA Sequence Affects Both Translocation and Unwinding PcrA Kinetics. Recent studies of SF1 helicase UvrD (40) and SF2 helicase Hel308 (14, 18, 19) have shown that ssDNA translocation speed can be strongly affected by the underlying DNA base composition. SPRNT is well suited to detection of sequence-dependent kinetics because SPRNT measures enzyme position by detecting the DNA sequence directly (*Materials and Methods*), thereby revealing an enzyme's sequence-specific position along the DNA strand. The long, repetitive DNA strand used in this study allowed for collection of data in which a single PcrA enzyme walks over the same 86-base-long DNA sequence multiple times at several different applied forces, allowing for accumulation of significant sequence-specific kinetic data. Fig. 4A shows the median dwell time for a forward step as a function of location within the 86-base-long repeat section of the antisense strand for both double-stranded DNA unwinding (T_{Unwind}) and ssDNA translocation (T_{Trans}) (sense

strand in *SI Appendix, Fig. S19*). For simplicity, dwell-times in which the eight separate linkers are within either the pore or PcrA are not shown; all measured dwell-times are shown in *SI Appendix, Fig. S20*. Average dwell times vary by an order of magnitude depending upon where PcrA is along the sequence for both unwinding and translocation.

By leveraging the underlying structure of our DNA substrate, we were able to determine that the variation in dwell time was due to different bases within the PcrA. In SPRNT, DNA bases are read at the pore constriction, which is separated by ~ 12 nucleotides from the motor enzyme. During force-assisting experiments, PcrA enters the linker region several nucleotides before the linker region enters the pore constriction. This separation serves as a natural experiment in which we can compare step dwell times while MspA passes over the tail end of the repeat section and PcrA walks over different linker sequences (*SI Appendix, Fig. S20*). Significant sequence-dependent effects begin ~ 15 to 20 nucleotides prior to the linker's entry into the pore constriction. This is similar to previous SPRNT results with Hel308 helicase, in which sequence-dependent effects were found to be due to two sites within Hel308 separated 17 and 20 nucleotides from the pore constriction (19).

While one might assume the work required to unwind DNA would dictate the rate of unwinding, our data indicate that the ssDNA translocation rate plays an important role in unwinding. Even though unwinding is considerably slower than translocation, at each location along the DNA strand, T_{Unwind} and T_{Trans} are correlated (Fig. 4B and *SI Appendix, Fig. S19*), suggesting that the rate-limiting reaction substep of DNA unwinding is coincident with a rate-limiting substep for translocation on ssDNA. In other words, the presence of the DNA duplex modifies the rate constants of the kinetic step in which domain 2A moves forward or backward (Fig. 2), rather than adding a new rate-limiting substep to the cycle. The work of unwinding the DNA duplex is performed as domain 2A advances, and the context of the ssDNA on which PcrA walks affects domain 2A's ability to advance into the DNA duplex. T_{Unwind} and T_{Trans} are correlated because many of the same binding energies contribute to the rates of both unwinding and translocation (*SI Appendix, Fig. S19D*).

The ratio of T_{Unwind} to T_{Trans} is often used to compare the difference between translocation and unwinding (5, 41, 42). If the ssDNA sequence alone fully determined the rate of DNA unwinding, we would expect this ratio to be flat over the 86-base-long region. Instead the ratio of T_{Unwind} to T_{Trans} also depends on the underlying sequence (Fig. 4C), implying that duplex identity also plays a role in determining sequence kinetics. Interestingly, the ratio of T_{Unwind} to T_{Trans} at 36 pN and at 28 pN assisting force shows similar sequence-dependent patterns (Fig. 4C), and the same pattern of sequence dependence is also apparent at 20 pN and 12 pN (*SI Appendix, Fig. S21*). This supports our conclusion that the assisting force has no effect on domain 2A motion in which unwinding occurs.

Fig. 4D shows a transition-state theory interpretation of this result for the substep in which domain 2A moves. In this model, the free energies of the bound states and transition state of the energy diagram are determined by the ssDNA sequence (Fig. 4D, solid line). Opposing force, be it DNA duplex or applied by SPRNT, modifies the energy landscape by increasing the transition state energy by some energy T and the bound-state energy by some energy E (Fig. 4D, dashed line). This approach suggests a more complicated relationship exists

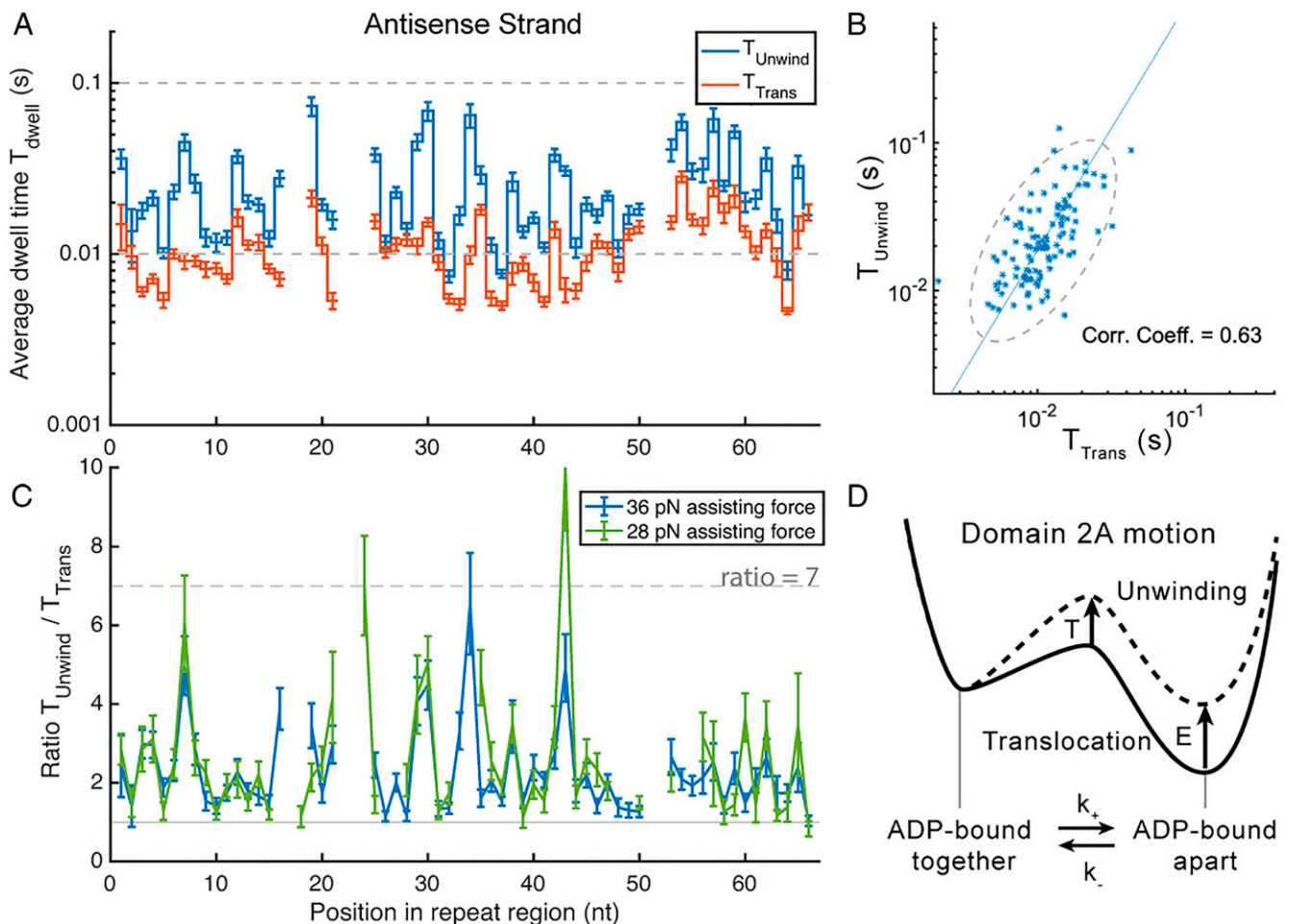


Fig. 4. (A) Average dwell time for a forward step for PcrA walking along the antisense strand during dsDNA unwinding (blue) and ssDNA translocation (orange) with 36 pN assisting force. The variation in dwell times as a function of position along the DNA indicates strong sequence dependence during translocation and unwinding. (B) Scatter plot of ssDNA T_{Trans} versus T_{Unwind} for both sense and antisense strand data on a log/log scale. (C) The ratio of T_{Unwind} to T_{Trans} as a function of location within the repeat section of the DNA antisense strand. The ratio in step dwell times is sequence dependent and consistent across different applied forces. Gaps within the data are in locations in which the ion-current trace has low signal to noise ratio and single nucleotide enzyme steps cannot be easily resolved. (D) Transition-state theory energy diagram showing how duplex unwinding modifies the forward and backward rates of domain 2A motion in the model in Fig. 2. Corr coeff, correlation coefficient.

between T_{Unwind} and T_{Trans} than simply $T_{\text{Unwind}} \propto T_{\text{Trans}}$ (*SI Appendix*, Fig. S19), because both the forward and backward rates of domain 2A motion are modified by force.

Discussion

SPRNT allows for direct observation of individual ATPase cycles of helicases, revealing fundamental mechanochemical substeps. By changing experimental conditions such as [ATP] and [ADP], and by applying assisting or opposing forces, we probed substeps of the inchworm mechanism to build a detailed picture of how PcrA unwinds DNA. As PcrA walks along ssDNA, the presence of a complementary DNA duplex exerts an opposing force which counters the advance of domain 2A. Larger opposing forces increase the backstepping rate of domain 2A, impeding forward progress. This backstepping is also ADP dependent; thus, unbinding of ADP helps to rectify PcrA's progress against an opposing force. SPRNT's ability to associate PcrA's steps with the underlying DNA sequence reveals a complex mechanochemical landscape for duplex unwinding that is dependent upon both the ssDNA sequence and the duplex stability. In this sense, PcrA is like a snowplow: the amount of snow in front of the plow is important but so too is the amount of traction available to the wheels.

Differences in base-pair stability vary how much work is required to unwind the DNA duplex, while the underlying ssDNA sequence significantly affects how quickly PcrA can perform that work. Sequence-dependent translocation kinetics should be investigated as a source of sequence-dependent unwinding behavior in other enzymes.

Our data show that the individual motion of both RecA domains, off-pathway stepping, and effects of DNA sequence on translocation and unwinding are all important details of PcrA kinetics. These details suggest that a full description of helicase behavior is far richer than models commonly used to describe helicase motion. Rather than existing on a spectrum from passive to active (5, 41, 42), PcrA exhibits a range of "activity" depending on both the ssDNA sequence and nucleotides being unwound.

The large variation in sequence-dependent stepping is significant when considering bulk average kinetic data such as average speed. The order-of-magnitude variation in step dwell times means that just a few steps that are slow because of their sequence contexts end up dominating PcrA's average behavior. This, in addition to static disorder, helps to explain the broad range of speeds measured. Characterizing PcrA by its average behavior misses important features that our SPRNT data are able to reveal. Our data cover a broad range of sequence

contexts (*SI Appendix, Figs. S3–S5*), suggesting that PcrA's kinetics depend on the underlying sequence in general and not just for one particular DNA sequence motif. Comparison of the T_{Unwind} to T_{Trans} ratio with the base-pairing binding energies of the underlying sequence does not reveal a simple relationship between a single base pair and the effect of the DNA duplex on unwinding speed (*SI Appendix, Fig. S22*). Also, base dimers (*SI Appendix, Fig. S23*), nearest neighbor pairs (*SI Appendix, Fig. S24*), and purine and pyrimidine content (*SI Appendix, Fig. S25*) cannot fully account for the nearly 10-fold variation observed in T_{Trans} and T_{Unwind} . Furthermore, T_{Trans} and T_{Unwind} have no apparent autocorrelation (*SI Appendix, Fig. S26*), as might be expected if sequence dependence were due to some local average quantity such as GC content or purine and pyrimidine content. This instead suggests that the observed sequence dependence is site specific, involving the interaction of specific bases with specific regions within PcrA and that several bases are involved. There are significant differences between our PcrA data and data obtained previously with Hel308 helicase. For example, Hel308 was weakly dependent upon the magnitude of opposing force, whereas PcrA is strongly force dependent. In Hel308, we found that nearly all rate constants for steps of the inchworm model were sequence dependent (19); it would be reasonable to expect the same to be true with PcrA. The crystal structure of PcrA reveals numerous contacts between the DNA duplex and the exterior of PcrA, suggesting that several DNA bases within the duplex may be important for determining unwinding speed. Systematic studies on additional sequence contexts, such as that performed previously with Hel308 helicase (19), will be needed to fully understand the cause of such sequence dependence.

The fact that sequence-dependent translocation has now been observed in three different SF1 and SF2 helicases [PcrA, Hel308 (19), and UvrD (40)] suggests that sequence dependence is a common behavior of helicases. That such sequence dependence has only recently been observed is unsurprising. It is difficult to detect such sequence dependence via ensemble measurements and, to date, many single-molecule studies used homopolymer DNA and studies using heterogeneous DNA sequences did not reveal the enzyme's sequence-specific location. Because SPRNT measures an enzyme's location by reading the DNA sequence, dwell times can be averaged as a function of DNA position, enabling detection of sequence-dependent phenomena.

Unlike protein filaments (e.g., actin), DNA is not a homogeneous track; sequence-dependent behavior may be the norm rather than the exception. Strong sequence-dependent enzyme kinetics such as those observed in our data likely affect PcrA's role in vivo and could thereby exert selective pressure on both DNA and protein evolution. Therefore, sequence-dependent behavior should be carefully considered in future studies of any enzyme that walks along DNA or RNA, since the sequence-dependent kinetics may reveal essential features of an enzyme's function. Such effects are almost certainly used by life to achieve various ends, and SPRNT is well suited to discovering how and why such sequence dependence occurs and opens the possibility of uncovering enzyme functions that were hereto unknown.

Materials and Methods

A single MspA pore is prepared in an unsupported phospholipid bilayer, as previously reported (15). The pore is prepared with asymmetric salt conditions to provide a low-salt environment for PcrA while still ensuring a strong ion-current signal. The *trans* well contains 500 mM KCl, 10 mM Hepes, buffered to pH 8.00 ± 0.05 , and the *cis* well contains 100 mM KCl, 10 mM MgCl_2 , 10 mM Hepes, and various [ATP] and [ADP], buffered to pH 8.00 ± 0.05 . Unless

otherwise noted, all experiments occur at room temperature. A voltage is applied across the membrane by an Axopatch 200B patch-clamp amplifier (Molecular Devices). Once an ss nucleic acid end is captured by the electric field in the pore, it is rapidly pulled through the pore until the bound motor enzyme contacts the rim of the nanopore. From this moment onward, the enzyme controls the motion of the nucleic acid through the pore, until the enzyme falls off the nucleic acid.

Data are acquired at a sampling rate of 50 kHz filtered with an 8-pole 10-kHz Bessel filter. Data are then digitally down-sampled to 5 kHz for analysis using a boxcar filter. Single-enzyme traces are detected automatically via thresholding. Reads begin when the current drops below 80% of the open pore current and end when the ion current returns to above 94% of open pore current for more than 10 data points. Putative events are then evaluated by hand by recognition of ion-current patterns corresponding to sense or antisense strand and 3' and 5' feeding (*SI Appendix, Figs. S3–S5*). The 5'-feeding antisense data are not used in this study because this DNA sequence produces a long region of low-current contrast, which interferes with detection of individual enzyme steps. Steps in ion-current data are detected using a change-point algorithm previously described (14, 18). Ion-current values are then automatically aligned to the corresponding ion-current consensus (*SI Appendix, Figs. S3–S5*) using a previously described dynamic-programming alignment algorithm (17). In this way, ion-current values are matched to their corresponding location within the DNA strand and sequence-specific step dwell times can be binned accordingly. If adjacent ion-current levels are aligned to the same consensus current level, their dwell times are combined. Error bars in the position versus time graph shown in Fig. 1F are the inverse signal to noise ratio (SNR) and represent the relative certainty with which a given level is aligned to that position. Unlike optical tweezers or magnetic tweezers, the SNR for SPRNT varies depending on the local ion-current contrast. Places in which ion current changes significantly with position (e.g., high slope in the spline of Fig. 1D) have high SNR, whereas places in which the ion current changes little with position (e.g., low slope in Fig. 1D) have lower SNR. For more details see ref. 15.

Varying forces are applied by changing the voltage applied across the membrane. DNA-enzyme complexes were captured at 180 mV and then switched at intervals to 60 mV, 100 mV, and 140 mV. Current estimates of applied force are 0.20 ± 0.04 pN/mV based on how DNA stretches within the pore at different applied forces (43). Applied voltages of 60 mV, 100 mV, 140 mV, and 180 mV correspond to 12 ± 2 pN, 20 ± 4 pN, 28 ± 6 pN, and 36 ± 7 pN, respectively. In comparison to the literature, these forces appear quite large, but the way in which the force is applied is key to how the applied force affects enzyme-stepping kinetics (12). All experiments were performed at room temperature.

WT PcrA is a poor helicase, only unwinding a few bases at a time; however, recent studies revealed that by constraining the conformation of PcrA's accessory domains into a "closed" configuration, PcrA could be transformed into a so-called super-helicase capable of unwinding thousands of bases at a time against large opposing forces (31). In this study, we use this activated PcrA helicase from *Geobacillus stearothermophilus* (accession no. P56255) with the mutations (C96A, C247A, N187C, and L409C) "PcrA-X." The use of chemically activated PcrA in this study enabled us to observe processive unwinding by a helicase using SPRNT. Without crosslinking into the closed form, these monomeric enzymes switch strands after unwinding just a few base pairs and translocate on the opposite strand while in the open form, letting the DNA rezip (44). This behavior plays a regulatory role by preventing unwinding of a long stretch of DNA until a partner protein comes and stabilizes the closed form (31). Ideally, crosslinking simply disables strand switching, thereby providing insight into the mechanism of processive unwinding. As noted by Arslan et al. (31), the chemical crosslinking that locks PcrA into the "closed" state required the removal of two natural cysteines (C96 and C247), which decreased ATPase activity when compared with WT PcrA. The crosslinking reaction itself does not seem to change ssDNA translocation, because control experiments on this PcrA mutant before chemical crosslinking showed similar translocation behavior (*SI Appendix, Fig. S27*).

PcrA helicase was purified and crosslinked as previously described (31). Briefly, we inserted the PcrA sequence between the NdeI and BamHI sites of the pET-11b vector and transformed it into *Escherichia coli* BL21(DE3) cells grown in terrific broth medium. When optical density at 600 nm reached 0.6, the protein overexpression was induced with 0.5 mM isopropyl β -D-1-thiogalactopyranoside.

The cells were incubated overnight at 18 °C and harvested by centrifugation at 10,000 × *g*. Our PcrA contains 6×His tag on its N terminus for nickel-nitrilotriacetic acid affinity column-based purification. The cell pellet was resuspended in a lysis buffer and cells were lysed with a sonicator. After binding PcrA to the nickel-nitrilotriacetic acid column and several washes, PcrA was eluted with 150 mM imidazole-containing buffer. PcrA concentration was kept below 4 mg/mL (~50 μM) to avoid aggregation.

Our PcrA mutant has two native cysteines (C96A and C247A) removed, while N187C and L409C are introduced for crosslinking. New C187 and C409 are crosslinked with 1,8-bismaleimido-diethyleneglycol [BM(PEG)2] to lock PcrA in the closed conformation and form PcrA-X. Optimal crosslinking condition is achieved at a PcrA concentration between 20 and 25 μM, with PcrA to BM(PEG) ratio of 1:5 (SI Appendix, Fig. S28).

The long, repetitive DNA strand was replicated within *E. coli* (DH5-α) in a pET28a plasmid vector. Original assembly of the repetitive DNA was as described previously (32). After purification using a Qiagen Maxiprep plasmid purification kit (Qiagen). The 64× repeat was then cleaved out of the plasmid using XbaI and HindIII. Simultaneously, the remainder of the pET28a plasmid was digested with DdeI and Fnu4HI producing numerous small DNA segments and one 6-kb-long repetitive target DNA. The 6-kb-long 64× repeat was then purified using SPRIselect beads (Beckman Coulter) at a 1 to 0.4 volume per volume ratio. Adapters (SI Appendix, Fig. S2) were preannealed and then ligated to the purified repeat DNA using T4 ligase.

Instantaneous enzyme speed (nt/s) is measured using the time to travel 15 nucleotides in consecutive increments yielding several speed measurements

for each single-molecule trace. Unless otherwise noted, step dwell times are for forward steps that happened after another forward step. This conditional step characterization was taken into account to ensure full ATP turnover for each step. In the model of Fig. 2, a forward step that follows a backstep would not have the same dwell-time distribution as forward steps that follow a backward step, since a step's initial conditions modify which states the enzyme passes through before finalizing the step (18). A "backstep" refers to backward steps occurred immediately after forward steps; consecutive backsteps were rare. See SI Appendix for further discussion.

Rep-X helicase was prepared as described previously (31). *E. coli* UvrD helicase was acquired from Quidel.

Data, Materials, and Software Availability. The MATLAB workspace data, including all data for this report, are uploaded to figshare and are available at the following link: <https://doi.org/10.6084/m9.figshare.16528515> (45).

ACKNOWLEDGMENTS. This work was supported by the NIH National Human Genome Research Institute (Grant number R01HG005115) and the National Institute of General Medical Sciences (Grant number R35GM122569). M.G. was supported by the Natural Sciences and Engineering Research Council of Canada Postdoctoral Fellowship.

Author affiliations: ^aDepartment of Physics, University of Washington, Seattle, WA 98195; and ^bDepartment of Physics, Johns Hopkins University, Baltimore, MD 21218

- S. S. Patel, K. M. Picha, Structure and function of hexameric helicases. *Annu. Rev. Biochem.* **69**, 651–697 (2000).
- M. R. Singleton, M. S. Dillingham, D. B. Wigley, Structure and mechanism of helicases and nucleic acid translocases. *Annu. Rev. Biochem.* **76**, 23–50 (2007).
- T. M. Lohman, E. J. Tomko, C. G. Wu, Non-hexameric DNA helicases and translocases: Mechanisms and regulation. *Nat. Rev. Mol. Cell Biol.* **9**, 391–401 (2008).
- A. M. Pyle, Translocation and unwinding mechanisms of RNA and DNA helicases. *Annu. Rev. Biophys.* **37**, 317–336 (2008).
- B. Sun, M. D. Wang, Single-molecule perspectives on helicase mechanisms and functions. *Crit. Rev. Biochem. Mol. Biol.* **51**, 15–25 (2016).
- S. S. Velankar, P. Soutlanas, M. S. Dillingham, H. S. Subramanya, D. B. Wigley, Crystal structures of complexes of PcrA DNA helicase with a DNA substrate indicate an inchworm mechanism. *Cell* **97**, 75–84 (1999).
- R. Roy, S. Hohng, T. Ha, A practical guide to single-molecule FRET. *Nat. Methods* **5**, 507–516 (2008).
- E. A. Abbondanzieri, W. J. Greenleaf, J. W. Shaevitz, R. Landick, S. M. Block, Direct observation of base-pair stepping by RNA polymerase. *Nature* **438**, 460–465 (2005).
- J. R. Moffitt, Y. R. Chemla, S. B. Smith, C. Bustamante, Recent advances in optical tweezers. *Annu. Rev. Biochem.* **77**, 205–228 (2008).
- S. Dumont *et al.*, RNA translocation and unwinding mechanism of HCV NS3 helicase and its coordination by ATP. *Nature* **439**, 105–108 (2006).
- J. Hilario, S. C. Kowalczykowski, Visualizing protein-DNA interactions at the single-molecule level. *Curr. Opin. Chem. Biol.* **14**, 15–22 (2010).
- M. A. Makurath, K. D. Whitley, B. Nguyen, T. M. Lohman, Y. R. Chemla, Regulation of Rep helicase unwinding by an auto-inhibitory subdomain. *Nucleic Acids Res.* **47**, 2523–2532 (2019).
- S. Hodeib *et al.*, A mechanistic study of helicases with magnetic traps. *Protein Sci.* **26**, 1314–1336 (2017).
- I. M. Derrington *et al.*, Subangstrom single-molecule measurements of motor proteins using a nanopore. *Nat. Biotechnol.* **33**, 1073–1075 (2015).
- A. H. Laszlo, I. M. Derrington, J. H. Gundlach, MspA nanopore as a single-molecule tool: From sequencing to SPRNT. *Methods* **105**, 75–89 (2016).
- E. A. Manrao *et al.*, Reading DNA at single-nucleotide resolution with a mutant MspA nanopore and phi29 DNA polymerase. *Nat. Biotechnol.* **30**, 349–353 (2012).
- A. H. Laszlo *et al.*, Decoding long nanopore sequencing reads of natural DNA. *Nat. Biotechnol.* **32**, 829–833 (2014).
- J. M. Craig *et al.*, Revealing dynamics of helicase translocation on single-stranded DNA using high-resolution nanopore tweezers. *Proc. Natl. Acad. Sci. U.S.A.* **114**, 11932–11937 (2017).
- J. M. Craig *et al.*, Determining the effects of DNA sequence on Hel308 helicase translocation along single-stranded DNA using nanopore tweezers. *Nucleic Acids Res.* **47**, 2506–2513 (2019).
- J. M. Craig, A. H. Laszlo, I. C. Nova, J. H. Gundlach, Modelling single-molecule kinetics of helicase translocation using high-resolution nanopore tweezers (SPRNT). *Essays Biochem.* **65**, 109–127 (2021).
- J. Park *et al.*, PcrA helicase dismantles RecA filaments by reeling in DNA in uniform steps. *Cell* **142**, 544–555 (2010).
- K. C. Lehmann, E. J. Snijder, C. C. Posthuma, A. E. Gorbalenya, What we know but do not understand about nidovirus helicases. *Virus Res.* **202**, 12–32 (2015).
- J. Yu, T. Ha, K. Schulten, Structure-based model of the stepping motor of PcrA helicase. *Biophys. J.* **91**, 2097–2114 (2006).
- M. S. Dillingham, P. Soutlanas, P. Wiley, M. R. Webb, D. B. Wigley, Defining the roles of individual residues in the single-stranded DNA binding site of PcrA helicase. *Proc. Natl. Acad. Sci. U.S.A.* **98**, 8381–8387 (2001).
- C. N. Merrikk, B. J. Brewer, H. Merrikk, The *B. subtilis* accessory helicase PcrA facilitates DNA replication through transcription units. *PLoS Genet.* **11**, e1005289 (2015).
- A. R. Mhashal, C. K. Choudhury, S. Roy, Probing the ATP-induced conformational flexibility of the PcrA helicase protein using molecular dynamics simulation. *J. Mol. Model.* **22**, 54 (2016).
- M. E. Fairman-Williams, U.-P. Guenther, E. Jankowsky, SF1 and SF2 helicases: Family matters. *Curr. Opin. Struct. Biol.* **20**, 313–324 (2010).
- M. R. Singleton, D. B. Wigley, Modularity and specialization in superfamily 1 and 2 helicases. *J. Bacteriol.* **184**, 1819–1826 (2002).
- J. Y. Lee, W. Yang, UvrD helicase unwinds DNA one base pair at a time by a two-part power stroke. *Cell* **127**, 1349–1360 (2006).
- M. S. Dillingham, Superfamily I helicases as modular components of DNA-processing machines. *Biochem. Soc. Trans.* **39**, 413–423 (2011).
- S. Arslan, R. Khafizov, C. D. Thomas, Y. R. Chemla, T. Ha, Protein structure. Engineering of a superhelicase through conformational control. *Science* **348**, 344–347 (2015).
- J. Zhang *et al.*, Tandem spinach array for mRNA imaging in living bacterial cells. *Sci. Rep.* **5**, 17295 (2015).
- M. S. Dillingham, D. B. Wigley, M. R. Webb, Demonstration of unidirectional single-stranded DNA translocation by PcrA helicase: Measurement of step size and translocation speed. *Biochemistry* **39**, 205–212 (2000).
- B. P. English *et al.*, Ever-fluctuating single enzyme molecules: Michaelis-Menten equation revisited. *Nat. Chem. Biol.* **2**, 87–94 (2006).
- V. I. Claessen *et al.*, Single-biomolecule kinetics: The art of studying a single enzyme. *Annu. Rev. Anal. Chem. (Palo Alto, Calif.)* **3**, 319–340 (2010).
- L. Edman, Z. Földes-Papp, S. Wennmalm, R. Rigler, The fluctuating enzyme: A single molecule approach. *Chem. Phys.* **247**, 11–22 (1999).
- A. Niedziela-Majka, M. A. Chesnik, E. J. Tomko, T. M. Lohman, *Bacillus stearothermophilus* PcrA monomer is a single-stranded DNA translocase but not a processive helicase in vitro. *J. Biol. Chem.* **282**, 27076–27085 (2007).
- D. Keller, C. Bustamante, The mechanochemistry of molecular motors. *Biophys. J.* **78**, 541–556 (2000).
- M. K. Levin, M. Gurjar, S. S. Patel, A Brownian motor mechanism of translocation and strand separation by hepatitis C virus helicase. *Nat. Struct. Mol. Biol.* **12**, 429–435 (2005).
- E. J. Tomko, T. M. Lohman, Modulation of *Escherichia coli* UvrD single-stranded DNA translocation by DNA base composition. *Biophys. J.* **113**, 1405–1415 (2017).
- M. D. Betterton, F. Jülicher, Opening of nucleic-acid double strands by helicases: Active versus passive opening. *Phys. Rev. E Stat. Nonlin. Soft Matter Phys.* **71**, 011904 (2005).
- M. Manosak, X. G. Xi, D. Bensimon, V. Croquette, Active and passive mechanisms of helicases. *Nucleic Acids Res.* **38**, 5518–5526 (2010).
- M. T. Noakes *et al.*, Increasing the accuracy of nanopore DNA sequencing using a time-varying cross membrane voltage. *Nat. Biotechnol.* **37**, 651–656 (2019).
- M. J. Comstock *et al.*, Protein structure. Direct observation of structure-function relationship in a nucleic acid-processing enzyme. *Science* **348**, 352–354 (2015).
- A. H. Laszlo *et al.*, Code and Dataset for "Sequence-dependent mechanochemical coupling of helicase translocation and unwinding at single-nucleotide resolution". figshare. <https://doi.org/10.6084/m9.figshare.16528515>. Deposited 18 August 2022.